Research Article



Superposition coded OFDM transmissions in a downlink cooperative relay network based on statistical channel state information

ISSN 1751-8628 Received on 8th December 2017 Revised 1st May 2018 Accepted on 5th January 2019 E-First on 4th February 2019 doi: 10.1049/iet-com.2018.5263 www.ietdl.org

Sharief Abdel-Razeq^{1 ∞}, Shengli Zhou¹, Zhengdao Wang², Ming Zhao³

¹Department of Electrical and Computer Engineering, University of Connecticut, Storrs, CT 06269, USA

⋈ E-mail: sharief.abdel-razeq@uconn.edu

Abstract: Non-orthogonal multiple access has recently emerged as a promising multiple access technique for future wireless technology. In this study, the authors investigate superposition coding in a downlink cooperative cellular system based on the orthogonal frequency division multiplexing (OFDM) modulation in the presence of frequency selective multipath fading channels, a setup that has not been studied before. Specifically, the base station communicates with two paired mobile users simultaneously via the OFDM modulation with the help of a half-duplex relay under either the decode-and-forward (DF) or amplify-and-forward (AF) scheme, where the power allocation between two mobile users depends on the statistical channel state information (CSI) rather than perfect CSI. They derive the ergodic rate regions under Rayleigh fading channels and present an *ad-hoc* approach to determine the power splitting parameters when the target data rates are given. Simulation results based on the outage probabilities show that superposition coding consistently outperforms frequency division, however, the relative advantage of the DF and AF schemes in a superposition-coded OFDM relay system depends on the system geometry.

1 Introduction

To achieve significant gains in capacity and quality of user experience, the research defining the fifth generation (5G) networks has received considerable attention [1-5]. The state-ofthe-art wireless communication systems have been utilising orthogonal multiple access (OMA) techniques, in which, the resources are allocated orthogonally to multiple users. These techniques include time-division multiple access (TDMA), frequency-division multiple access (FDMA), orthogonal frequency-division multiple access (OFDMA), and code-division multiple access (CDMA), where multiple users are multiplexed in the time, frequency, or code domains, respectively. Recently, as a major candidate of multiple access technique in the 5G mobile communication system, non-orthogonal multiple access (NOMA) have received significant attention for 5G cellular networks, thanks to ability of serving multiple users using the same time and frequency resources.

There are two main categories of NOMA techniques based on power-domain and code-domain user separations [6]. In this paper, we focus on the power-domain NOMA in the form of superposition coding (SC). In a two-user setting, the transmitter transmits signals to two users simultaneously with different power levels. The user with a lower channel gain considers the signal of the other user as noise and detects its own signal directly. The user with a larger channel gain performs successive interference cancellation (SIC), i.e. this user detects and subtracts the signal of the other user, and then proceeds to decode its own signal [6, 7]. There are extensive investigations on superposition coded systems. For our convenience, we next divide existing works into four categories depending on the channel and system setups. We first consider flatfading channels and describe superposition coded systems in noncooperative and cooperative systems. We then consider frequency selective channels and describe superposition coded OFDM transmissions in noncooperative and cooperative systems.

1.1 Superposition coding in non-cooperative systems

Superposition coding was proposed in [8, 9] for single-antenna downlink cellular systems, where NOMA is shown to be superior than OMA in terms of the overall cell throughput and cell-edge user throughput in both low and high mobility scenarios. In [10], the conditions under which the spectral efficiency gains of NOMA are guaranteed compared to OMA are derived for each individual user in both uplink and downlink. Furthermore, the extension to multiple-input multiple-output (MIMO) systems has been extensively studied in [11–19]. The results collectively demonstrated that MIMO-NOMA outperforms conventional MIMO-OMA.

1.2 Superposition coding in cooperative systems

Cooperative relaying systems (CRS) provide the destination an opportunity to receive and combine two independent copies of the same data from the source via the direct and relayed channels to improve the overall system performance [20]. Application of superposition coding in a relay system comes in two forms: (i) assigning one NOMA user to act as a relay for other users, or (ii) employing a dedicated relay to assist all users.

In the first category, it was shown in [21] that the performance of cooperative NOMA is always superior to cooperative OMA. Cooperative MIMO-NOMA was studied in [22] where intra-beam SC at the transmitter and inter-beam SIC at the receiver are proposed for the users within a beam.

In the second category, various scenarios with different numbers of transmitters and receivers have been studied using different forwarding schemes such as the decode-and-forward (DF) and the amplify-and-forward (AF) [23–31]. In particular, the exact and asymptotic expressions for the achievable average rate in independent Rayleigh fading channels were derived in [23]. The outage behaviour and the ergodic sum rate of the two paired users have been presented in [25] and the problem of relay selection has been studied in [27]. In both categories, it was shown in [32–34] that the spectral efficiency of cooperative NOMA can be further

²Department of Electrical and Computer Engineering, Iowa State University, Ames, IA 50011, USA

³Department of Electronic Engineering and Information Science, University of Science and Technology of China, Hefei, Anhui 230027, People's Republic of China

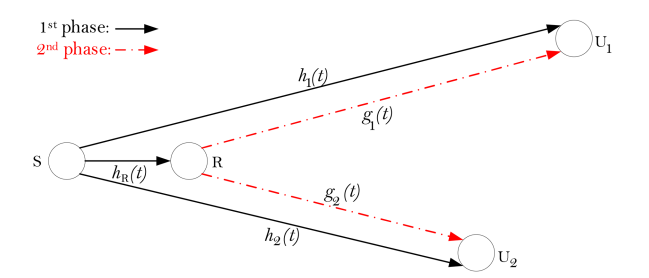


Fig. 1 Downlink NOMA in a cooperative relay network (R could be placed at different locations)

improved by employing a full-duplex cooperation mechanism instead of a half-duplex one.

1.3 Superposition coded OFDM in non-cooperative systems

Broadband wireless systems encounter frequency selective multipath fading channels. Orthogonal frequency division multiplexing (OFDM) prevails in recent wireless standards such as wireless fidelity (WiFi) and 4G cellular systems due to its ability to handle long dispersive channels. In addition to OFDM, there are several 5G waveform candidates, such as universal filtered multicarrier (UFMC), filter bank multicarrier (FBMC), and generalised frequency division multiplexing (GFDM). Each waveform has its own characteristics and the comparison among these waveforms is an interest subject; see e.g. [35-37]. Such a comparison is out of the scope of this paper. It was shown in [38] that a NOMA-OFDM system can further enhance the spectral efficiency as well as accommodate more users compared with the conventional OFDMA system. The resource allocation (RA) problem for a downlink NOMA-OFDM system was investigated in [39, 40]. An algorithm to optimally minimise the total transmit power for a given quality of service (QoS) requirements was provided in [39] under the assumption that perfect channel state information (CSI) is available at both the transmitter and receivers. Ma et al. [41] presented a practical superposition coded OFDM scheme for an underwater acoustic communication system with statistical CSI at the transmitter. Further, superposition coding has been applied to reduce the peak-to-average power ratio (PAPR) of OFDM transmissions in [42].

1.4 Superposition coded OFDM in co-operative systems

In this paper, we study superposition coded OFDM transmissions in a downlink cooperative relay system. It's worth to mention that OFDM transmissions has large PAPRs. However, the PAPR issue is less of concern for the base station as compared to the user equipment, and OFDM transmissions are currently used in 4G cellular downlink. To the best of our knowledge, there is no existing work on this topic. We consider a practical scenario where the power is allocated to two users based on the statistical CSI available at the transmitters. We derive the ergodic rate regions and present an ad-hoc approach to determine the power splitting parameters when the target data rates are given. Simulation results show that superposition coding outperforms frequency division (FD) consistently regardless the system geometry and the relay scheme. However, the relative advantage of the DF and AF schemes in the context of superposition coded OFDM depends on the system geometry.

The remaining of this paper is organised as follows. Section 2 introduces the system setup and main assumptions. Sections 3 and 4 present the DF and AF schemes, respectively, then analyse them in terms of ergodic rate and outage probability. Section 5 compares the performance of the DF, AF and no-relay (NR) schemes in the context of superposition coded OFDM transmissions. Finally, Section 6 concludes this paper.

2 System setup

Consider a downlink cooperative scenario, where one source node S intends to transmit information to multiple distant users with the

help of a relay R and the direct links between S and these users exist. One practical way of limiting the system complexity is to break the users into groups, with each group containing two users with disparate channels [43]. Across the user groups, transmissions are kept orthogonal via frequency division or time division. Hence, we explicitly study a two-user case in this paper, where two users are labelled as U_1 (The far user) and U_2 (The near user), as shown in Fig. 1. We assume that all the nodes are single-antenna devices and operate in a half-duplex mode. The delivery of information to these two users will be done in two consecutive phases. In the first phase, S broadcasts a signal $x_s(t)$ whereas R, U_1 , and U_2 listen. In the second phase, R broadcasts a relay signal $x_R(t)$ to U_1 and U_2 , where either the DF or AF scheme will be used.

There are five channels involved in the system setup. Let $h_{\rm R}(t)$, $h_1(t)$, $h_2(t)$ denote the S-to-R, S-to- U_1 , and S-to- U_2 channels, respectively, and let $g_1(t)$, $g_2(t)$ denote the R-to- U_1 and R-to- U_2 channels, respectively. All the involved channels are assumed frequency selective, and OFDM modulation is used for data transmission on all the links. To facilitate the discussion, we next provide a brief description of OFDM.

2.1 OFDM

Assume that a cyclic-prefix (CP) OFDM block transmission is used, where the system parameters include the bandwidth B, the total number of subcarriers K, the symbol duration T, and a CP of length $T_{\rm cp}$. The subcarrier spacing is then $\Delta f = B/K$. Let x[k] denote the data symbol transmitted at the kth subcarrier during an OFDM block. The time-domain waveform can be expressed as

$$x(t) = \sum_{k \in K} x[k] e^{j2\pi k\Delta ft}, \quad t \in [-T_{cp}, T].$$
 (1)

After passing through a frequency selective channel h(t), the received signal is

$$y(t) = h(t) \star x(t) + \eta(t), \tag{2}$$

where \star stands for convolution and $\eta(t)$ is the additive noise. The receiver performs Fourier transform to obtain the frequency-domain samples

$$y[k] = \frac{1}{T} \int_0^T y(t) e^{-j2\pi k \Delta f t} dt.$$
 (3)

Let H[k] denote the channel frequency response at the kth subcarrier

$$H[k] = \int h(t)e^{-j2\pi k\Delta ft} dt,$$
 (4)

whose average power reflects the channel strength as

$$\mathbb{E}\left[H[k]^{2}\right] = \mathbb{E}\left[\int\left|h(t)\right|^{2} dt\right]. \tag{5}$$

The superiority of OFDM modulation is that it establishes the following channel input-output relationship in the frequency domain

$$y[k] = H[k]x[k] + \eta[k], \quad k = 0, ..., K - 1,$$
 (6)

where $\eta[k]$ is the additive noise sample. Out of K parallel subcarriers, there are K_p pilot subcarriers that carry known symbols to enable channel estimation at the receiver and K_d data subcarriers to carry the user payload. In this paper, we assume perfect channel estimation at the receiver and investigate the performance limit of various data transmission scenarios.

2.2 Channel model and statistical CSI

Based on the OFDM modulation, we now spell out the channel models for the five links involved in the system. At the end of the first phase, the received signals at R, U_1 , and U_2 at each subcarrier k = 0, ..., K - 1 are given by

$$y_{R}[k] = H_{R}[k]x_{S}[k] + \eta_{R}[k],$$
 (7)

$$y_1[k] = H_1[k]x_S[k] + \eta_1[k],$$
 (8)

$$y_2[k] = H_2[k]x_S[k] + \eta_2[k],$$
 (9)

where the noise samples are Gaussian distributed as $\eta_R[k] \sim \mathcal{N}(0, \sigma_R^2)$, $\eta_1[k] \sim \mathcal{N}(0, \sigma_1^2)$, and $\eta_2[k] \sim \mathcal{N}(0, \sigma_2^2)$. At the end of the second phase, the received signals at U_1 and U_2 are

$$\tilde{y}_1[k] = G_1[k]x_R[k] + \tilde{\eta}_1[k],$$
 (10)

$$\tilde{y}_2[k] = G_2[k]x_R[k] + \tilde{\eta}_2[k],$$
 (11)

where the noise samples are Gaussian distributed as $\tilde{\eta}_1[k] \sim \mathcal{N}(0, \tilde{\sigma}_1^2)$ and $\tilde{\eta}_2[k] \sim \mathcal{N}(0, \tilde{\sigma}_2^2)$.

For simplicity, we assume that the noise levels are the same at R, U_1 , and U_2 , i.e. $\sigma^2 = \sigma_R^2 = \sigma_i^2 = \tilde{\sigma}_i^2$, i = 1, 2. Let P_S and P_R denote the symbol energy on each OFDM subcarrier for S and R transmissions, respectively. The instantaneous signal-to-noise ratios (SNRs) and their average values are defined as follows:

$$\gamma_{R}[k] = \frac{|H_{R}[k]|^{2} P_{S}}{\sigma^{2}}, \quad \Gamma_{R} = \mathbb{E}\{\gamma_{R}[k]\},
\gamma_{I}[k] = \frac{|H_{I}[k]|^{2} P_{S}}{\sigma^{2}}, \quad \Gamma_{I} = \mathbb{E}\{\gamma_{I}[k]\},
\gamma_{2}[k] = \frac{|H_{2}[k]|^{2} P_{S}}{\sigma^{2}}, \quad \Gamma_{2} = \mathbb{E}\{\gamma_{2}[k]\},
\tilde{\gamma}_{I}[k] = \frac{|G_{I}[k]|^{2} P_{R}}{\sigma^{2}}, \quad \tilde{\Gamma}_{I} = \mathbb{E}\{\tilde{\gamma}_{I}[k]\},
\tilde{\gamma}_{2}[k] = \frac{|G_{2}[k]|^{2} P_{R}}{\sigma^{2}}, \quad \tilde{\Gamma}_{2} = \mathbb{E}\{\tilde{\gamma}_{2}[k]\}.$$
(12)

In this paper, we assume that S and R have the knowledge of the average SNRs of all links, i.e. $\{\tilde{\Gamma}_1, \tilde{\Gamma}_2, \Gamma_R, \tilde{\Gamma}_1, \tilde{\Gamma}_2\}$ to optimise their transmissions. This is in contrast with existing works [44–46], where perfect CSI is assumed at the transmitters. In practical systems, the channels could be fast varying, but the channel statics can remain constant for a long period so that they can be fed back to assist the system optimisation [41].

2.3 Superposition coding

Superposition coding is a non-orthogonal scheme for downlink communications which has been recently proposed for 3rd generation partnership project long-term evolution advanced (3GPP-LTE-A) cellular networks in Release 14 [47, 48]. In SC, all users are allowed to access the channel freely and SIC is used for decoding [49, 50]. For the two-user case, the symbol transmitted at S is

$$x_{\rm S}[k] = \sqrt{\alpha P_{\rm S}} x_1[k] + \sqrt{\bar{\alpha} P_{\rm S}} x_2[k],\tag{13}$$

where $x_1[k]$ and $x_2[k]$ are the information symbols transmitted to U_1 and U_2 at the kth subcarrier, $\alpha \in [0,1]$ is the power fraction assigned to U_1 , and $\bar{\alpha} = 1 - \alpha$. For notational convenience, the transmitted symbols $x_1[k]$ and $x_2[k]$ are assumed to have unit average energy.

For the AF scheme, R simply forwards the received signal after proper amplification. However, for the DF scheme, R needs first to decode both the data streams and then applies SC again, but with a different power allocation as

$$x_{\rm R}[k] = \sqrt{\beta P_{\rm R}} x_{\rm I}[k] + \sqrt{\bar{\beta} P_{\rm R}} x_{\rm 2}[k], \tag{14}$$

where $\beta \in [0, 1]$ is the power fraction assigned to U_1 and $\bar{\beta} = 1 - \beta$. If R cannot decode the transmitted symbols correctly, no transmission occurs, and P_R will be set to zero.

Next, we will examine the receiver design and system performance of the DF and AF schemes separately.

3 Decode and forward

In this section, we study the scenario where R applies the DF scheme. During the first phase, R will decode $x_1[k]$ and $x_2[k]$ based on the received signal $y_R[k]$. As U_2 is the near user to S and hence has a larger SNR than U_1 , R first decodes $x_1[k]$ by treating $x_2[k]$ as interference, performs SIC, and then decodes $x_2[k]$ [41]. In the second phase, R will forward the decoded symbols with power P_R to the destinations.

The decoding order is done per subcarrier, instead of jointly across all data subcarriers, as the data symbols are assumed to be interleaved. Under this assumption, the far user U_1 has the received signals.

$$y_1[k] = H_1[k](\sqrt{\alpha P_S} x_1[k] + \sqrt{\bar{\alpha} P_S} x_2[k]) + \eta_1[k],$$
 (15)

$$\tilde{y}_1[k] = G_1[k](\sqrt{\beta P_R} x_1[k] + \sqrt{\bar{\beta} P_R} x_2[k]) + \tilde{\eta}_1[k].$$
 (16)

To combine the received signals, we adopt the maximum ratio combining (MRC) where the weights are proportional to the individual SNRs on each branch with the goal of maximising the SNR at the output of MRC detector [51, 52].

$$z_1[k] = w_{11}[k]y_1[k] + w_{12}[k]\tilde{y}_1[k], \tag{17}$$

where $w_{11}[k]$ and $w_{12}[k]$ are the weights. Since U_1 will decode its own data $x_1[k]$ in the presence of interference from U_2 's signal, i.e. $x_2[k]$ is treated as another source of additive noise and the weights can be specified as

$$w_{11}[k] = \frac{\sqrt{\alpha P_{\rm S}} H_1^*[k]}{\bar{\alpha} P_{\rm S} |H_1[k]|^2 + \sigma^2},\tag{18}$$

$$w_{12}[k] = \frac{\sqrt{\beta P_{\rm R}} G_1^*[k]}{\bar{\beta} P_{\rm R} |G_1[k]|^2 + \sigma^2}.$$
 (19)

The instantaneous signal-to-noise-plus-interference ratio (SINR) at U_1 will be

$$\gamma_{1}^{\text{DF}}[k] = \frac{\alpha P_{\text{S}} |H_{1}[k]|^{2}}{\bar{\alpha} P_{\text{S}} |H_{1}[k]|^{2} + \sigma^{2}} + \frac{\beta P_{\text{R}} |G_{1}[k]|^{2}}{\bar{\beta} P_{\text{R}} |G_{1}[k]|^{2} + \sigma^{2}}$$
(20)

$$= \frac{\alpha}{\bar{\alpha} + \frac{1}{\gamma_1[k]}} + \frac{\beta}{\bar{\beta} + \frac{1}{\bar{\gamma}_1[k]}}.$$
 (21)

Hence, the instantaneous mutual information between S and U_1 at the kth subcarrier is

$$\mathcal{J}_{1}[k] = \frac{1}{2} \log_{2} \left(1 + \gamma_{1}^{DF}[k] \right)$$

$$= \frac{1}{2} \log_{2} \left(1 + \frac{\alpha}{\bar{\alpha} + \frac{1}{\gamma_{1}[k]}} + \frac{\beta}{\bar{\beta} + \frac{1}{\bar{\gamma}_{1}[k]}} \right). \tag{22}$$

The constant $\frac{1}{2}$ in (22) is due to the fact the total transmission time is split into two halves for both the DF and AF schemes. For the No-Relay scheme, this constant is removed.

Now let us look at the near user. The near user U_2 will detect U_1 's message $x_1[k]$ and, if decoding was successful, he will then remove it from the observation

$$y_2^{\Delta}[k] = y_2[k] - \sqrt{\alpha P_s} H_1[k] x_1[k] = \sqrt{\alpha P_s} H_2[k] x_2[k] + \eta_s[k],$$
(23)

$$\tilde{y}_{2}^{\Delta}[k] = \tilde{y}_{2}[k] - \sqrt{\beta P_{R}} G_{2}[k] x_{1}[k]
= \sqrt{\beta P_{R}} G_{2}[k] x_{2}[k] + \tilde{\eta}_{2}[k].$$
(24)

After finishing the two phases, the combined signal at the detector's output is

$$z_{2}[k] = w_{21}[k] y_{2}^{\Delta}[k] + w_{22}[k] \tilde{y}_{2}^{\Delta}[k], \tag{25}$$

where the weights are

$$w_{21}[k] = \frac{\sqrt{\bar{\alpha}P_8}H_2^*[k]}{\sigma^2},$$
 (26)

$$w_{22}[k] = \frac{\sqrt{\bar{\beta}P_{\rm R}}G_2^*[k]}{\sigma^2} \,. \tag{27}$$

The instantaneous SNR at U_2 is

$$\gamma_2^{\text{DF}}[k] = \frac{\bar{\alpha} P_{\text{S}} |H_2[k]|^2}{\sigma^2} + \frac{\bar{\beta} P_{\text{R}} |G_2[k]|^2}{\sigma^2}$$
 (28)

$$= \bar{\alpha} \gamma_2[k] + \bar{\beta} \tilde{\gamma}_2[k]. \tag{29}$$

Hence, the instantaneous mutual information between S and U_2 at the kth subcarrier is

$$\mathcal{I}_{2}[k] = \frac{1}{2}\log_{2}(1 + \gamma_{2}^{DF}[k])$$

$$= \frac{1}{2}\log_{2}(1 + \bar{\alpha}\gamma_{2}[k] + \bar{\beta}\tilde{\gamma}_{2}[k]).$$
(30)

Once we have the instantaneous mutual information between S and U_i at the kth subcarrier, the mutual information averaged over all data subcarriers can be found as

$$\mathcal{J}_i = \frac{1}{K_d} \sum_{k \in K_d} \mathcal{J}_i[k] \,. \tag{31}$$

We next carry out some further analysis of the ergodic rate. In the analysis, in order to obtain a performance benchmark, we assume that R always works. We then analyse the outage probabilities, where the outage at R is accounted for.

3.1 Average mutual information for U_1

Under the assumption that the subcarrier gains $|H_i[k]|$ and $|G_j[k]|$ undergo Rayleigh fading, the instantaneous SNRs will be exponentially distributed as follows:

$$f(\gamma_i) = \frac{1}{\Gamma_i} e^{-(\gamma_i/\Gamma_i)},$$

$$f(\tilde{\gamma}_i) = \frac{1}{\tilde{\Gamma}_i} e^{-(\gamma_i/\tilde{\Gamma}_i)},$$
(32)

where Γ_i and $\tilde{\Gamma}_i$ are the average SNRs. The average mutual information for U_i will be

$$\bar{\mathcal{J}}_i = \mathbb{E}[\mathcal{J}_i] = \mathbb{E}[\mathcal{J}_i[k]]. \tag{33}$$

For U_1 , the average mutual information is then

$$\bar{\mathcal{J}}_{1} = \mathbb{E}[\mathcal{J}_{1}] = \frac{1}{2\ln 2} \mathbb{E}\left[\ln\left(1 + \frac{\alpha}{\bar{\alpha} + \frac{1}{\gamma_{1}}} + \frac{\beta}{\bar{\beta} + \frac{1}{\bar{\gamma}_{1}}}\right)\right]. \tag{34}$$

For notational convenience, define

$$A = \frac{\alpha}{\tilde{\alpha} + (1/\gamma_1)}, \quad B = \frac{\beta}{\tilde{\beta} + (1/\tilde{\gamma}_1)}.$$
 (35)

Based on the identity

$$\ln(x) = \int_0^\infty \frac{1}{y} (e^{-y} - e^{-xy}) \, dy, \tag{36}$$

we obtain

$$\bar{\mathcal{J}}_{1} = \frac{1}{2\ln 2} \mathbb{E} \Big[\int_{0}^{\infty} \frac{1}{y} (e^{-y} - e^{-(1+A+B)y}) dy \Big]. \tag{37}$$

From the fact that the two channels are independent, we reach at

$$\bar{\mathcal{J}}_{1} = \frac{1}{2\ln 2} \int_{0}^{\infty} \frac{1}{y} (e^{-y} - e^{-y} \mathbb{E}[e^{-Ay}] \mathbb{E}[e^{-By}]) \, dy.$$
 (38)

Now, we need to deal with the two expectations in the integration, $\mathbb{E}[e^{-Ay}]$ and $\mathbb{E}[e^{-By}]$. Based on (32) and (33), we have

$$\mathbb{E}\left[e^{-Ay}\right] = \frac{1}{\Gamma_1} \int_0^\infty e^{\left(-\frac{ay}{\tilde{a} + \frac{1}{\gamma_1}}\right)} e^{-\frac{\gamma_1}{\Gamma_1}} d\gamma_1, \tag{39}$$

$$\mathbb{E}\left[e^{-By}\right] = \frac{1}{\widetilde{\Gamma}_{1}} \int_{0}^{\infty} e^{\left(-\frac{\beta y}{\widetilde{\beta} + \frac{1}{\widetilde{\Gamma}_{1}}}\right)} e^{-\frac{\widetilde{\gamma}_{1}}{\widetilde{\Gamma}_{1}}} d\widetilde{\gamma}_{1}. \tag{40}$$

Inserting (39) and (40) into (38), we get the average mutual information $\bar{\mathcal{J}}_1$. A two-dimensional integration is needed for numerical evaluations.

3.2 Average mutual information for U_2

We now derive a closed-form expression for the average mutual information for U_2 . We have

$$\bar{\mathcal{J}}_2 = \mathbb{E}[\mathcal{J}_2] = \frac{1}{2\ln 2} \mathbb{E} \left[\ln(1 + \bar{\alpha}\gamma_2 + \bar{\beta}\tilde{\gamma}_2) \right]. \tag{41}$$

The probability density function (pdf) of the sum of two independent random variables $Z = \bar{\alpha}\gamma_2 + \bar{\beta}\tilde{\gamma}_2$ can be found by convolving the individual pdfs as

$$f_{Z}(z) = \left[\frac{1}{\bar{\alpha}\Gamma_{2} - \bar{\beta}\tilde{\Gamma}_{2}} \left(e^{-\frac{z}{\bar{\alpha}\Gamma_{2}}} - e^{-\frac{z}{\bar{\beta}\tilde{\Gamma}_{2}}}\right)\right] U(z), \tag{42}$$

where $U(\,\cdot\,)$ represents the unit step function. Further carrying out the integration, we have

$$\bar{\mathcal{J}}_{2} = \frac{\bar{\beta}\tilde{\Gamma}_{2}e^{\frac{1}{\bar{\beta}\tilde{\Gamma}_{2}}}E_{i}(-\frac{1}{\bar{\beta}\tilde{\Gamma}_{2}}) - \bar{\alpha}\Gamma_{2}e^{\frac{1}{\bar{\alpha}\tilde{\Gamma}_{2}}}E_{i}(-\frac{1}{\bar{\alpha}\Gamma_{2}})}{2\ln 2(\bar{\alpha}\Gamma_{2} - \bar{\beta}\tilde{\Gamma}_{2})},$$
(43)

where $E_i(\cdot)$ is the exponential integral and defined as $E_i(x) = \int_{-\infty}^x \frac{e^t}{t} dt$ [53].

3.3 The boundary of the achievable ergodic rate region

For a given pair of (α, β) , we have found the average mutual information for U_1 and U_2 in Sections 3.1 and 3.2, respectively. This average mutual information specifies the theoretic limit when the codeword is long or when K approaches infinity. The ergodic rate region is then given by

$$\left\{ \bigcup \left[R_1 \le \bar{\mathcal{J}}_1, R_2 \le \bar{\mathcal{J}}_2 \right] \right\},\tag{44}$$

where the boundary of the achievable rate region can be obtained by varying the values of α and β .

3.4 Outage probability for a given rate pair

For a finite *K*, we look for the outage probability defined as

$$p_i^{\text{out}}(R_i^*) = \mathbb{P}\{\mathcal{F}_i < R_i^*\},\tag{45}$$

where R_i^* is the target rate for U_i .

In an ideal scenario, R will perfectly decode and forward all received data to the two users. However, this is not the case in a real scenario. To discuss this more, let us define three outage events; A, B, and C at R, U_1 , and U_2 , respectively.

The outage at R is declared if it cannot decode perfectly either U_1 's data or U_2 's data and hence remains idle and sets $P_R = 0$ for that period of time. The outage probability at R can be expressed as

$$\mathbb{P}(A) = 1 - \mathbb{P}\left\{\frac{1}{K_{d}} \sum_{k \in K_{d}} \frac{1}{2} \log_{2}\left(1 + \frac{\alpha \gamma_{R}[k]}{1 + \bar{\alpha} \gamma_{R}[k]}\right) \ge R_{1}^{*}\right\}$$

$$\left(1 + \frac{1}{K_{d}} \sum_{k \in K_{d}} \frac{1}{2} \log_{2}\left(1 + \bar{\alpha} \gamma_{R}[k]\right) \ge R_{2}^{*}\right\}.$$
(46)

For U_1 , the outage depends on the status of R as follows:

• If R is in outage, then

$$\mathbb{P}(\mathbf{B} \middle| \mathbf{A}) = \mathbb{P} \Big\{ \frac{1}{K_{d}} \sum_{k \in K_{d}} \frac{1}{2} \log_{2} \Big(1 + \gamma_{1}^{NR}[k] \Big) < R_{1}^{*} \Big\}, \tag{47}$$

where

$$\gamma_{\rm i}^{\rm NR}[k] = \frac{\alpha P_{\rm S} |H_{\rm i}[k]|^2}{\tilde{\alpha} P_{\rm S} |H_{\rm i}[k]|^2 + \sigma^2}.$$

• If R decodes perfectly, then

$$\mathbb{P}(\boldsymbol{B} \middle| \overline{\boldsymbol{A}}) = \mathbb{P}\left\{\frac{1}{K_{\text{d}}} \sum_{k \in K_{\text{d}}} \frac{1}{2} \log_2 \left(1 + \gamma_1^{\text{DF}}[k]\right) < R_1^*\right\},\tag{48}$$

where $\gamma_1^{DF}[k]$ is given by (20).

This way, the outage probability at U_1 is [54]

$$p_1^{\text{out}}(R_1^*) = \mathbb{P}(\boldsymbol{B}|\boldsymbol{A})\mathbb{P}(\boldsymbol{A}) + \mathbb{P}(\boldsymbol{B}|\overline{\boldsymbol{A}})\mathbb{P}(\overline{\boldsymbol{A}}). \tag{49}$$

For U_2 , the outage depends on the status of R as follows:

• If R is in outage, then

$$\mathbb{P}(C|A) = 1 - \mathbb{P}\left\{\frac{1}{K_{d}} \sum_{k \in K_{d}} \frac{1}{2} \log_{2}(1 + \gamma_{1 \to 2}^{NR}[k]) \ge R_{1}^{*}\right\}$$

$$\bigcap \frac{1}{K_{d}} \sum_{k \in K_{d}} \frac{1}{2} \log_{2}(1 + \gamma_{2}^{NR}[k]) \ge R_{2}^{*},$$
(50)

where

$$\gamma_{1\to 2}^{NR}[k] = \frac{\alpha P_{S}|H_{2}[k]|^{2}}{\bar{\alpha}P_{S}|H_{2}[k]|^{2} + \sigma^{2}}, \quad \gamma_{2}^{NR}[k] = \frac{\bar{\alpha}P_{S}|H_{2}[k]|^{2}}{\sigma^{2}}.$$
 (51)

• If R decodes perfectly, then

$$\mathbb{P}(C|\overline{A}) = 1 - \mathbb{P}\left\{\frac{1}{K_{d}} \sum_{k \in K_{d}} \frac{1}{2} \log_{2}(1 + \gamma_{1 \to 2}^{DF}[k]) \ge R_{1}^{*}\right\}$$

$$\bigcap \frac{1}{K_{d}} \sum_{k \in K_{d}} \frac{1}{2} \log_{2}(1 + \gamma_{2}^{DF}[k]) \ge R_{2}^{*},$$
(52)

where $\gamma_2^{DF}[k]$ is given by (28) and

$$\gamma_{1 \to 2}^{\mathrm{DF}}[k] = \frac{\alpha P_{\mathrm{S}} |H_2[k]|^2}{\bar{\alpha} P_{\mathrm{S}} |H_2[k]|^2 + \sigma^2} + \frac{\beta P_{\mathrm{R}} |G_2[k]|^2}{\bar{\beta} P_{\mathrm{R}} |G_2[k]|^2 + \sigma^2}.$$
 (53)

The outage probability at U_2 is then

$$p_2^{\text{out}}(R_2^*) = \mathbb{P}(C|A)\mathbb{P}(A) + \mathbb{P}(C|\overline{A})\mathbb{P}(\overline{A}). \tag{54}$$

Further analysis for outage probability is challenging due to the correlation among data subcarriers. Numerical simulation is hence adopted to evaluate the outage probability, where the outage at R is included.

3.5 System operation

We now consider system operation. The knowledge of $\{\Gamma_1, \Gamma_2, \Gamma_R, \tilde{\Gamma}_1, \tilde{\Gamma}_2\}$ is available at S and R. Now the system needs to support the target rates R_1^* and R_2^* , what should the system choose the parameters (α, β) ? Ideally, one would choose the parameters so that the two users experience the same outage probability. However, this probability cannot be easily predicted.

Here we adopt an *ad-hoc* approach to find (α, β) using the results from the ergodic rate region. Let $\lambda = R_2^*/R_1^*$ denote the target rate ratio, which determines the target operating point. With the knowledge of statistical CSI, the power fraction under the given target rate pair which achieves the ergodic rates is obtained according to

$$(\hat{\alpha}_{DF}, \hat{\beta}_{DF}) = \arg \min_{\alpha, \beta} \left| \frac{\bar{R}_2}{\bar{R}_1} - \lambda \right|,$$
 (55)

where (\bar{R}_1, \bar{R}_2) is the point on the boundary of the ergodic rate region.

4 Amplify and forward

In this section, we investigate the AF scheme. Due to the large number of data subcarriers, the received signal is assumed to have an almost constant power, hence, the amplification factor A_f is a constant and given by

$$A_f = \frac{\sqrt{P_R}}{\sqrt{P_S \mathbb{E}[\left|H_R[k]\right|^2] + \sigma^2}}.$$
 (56)

Therefore

$$x_{\mathsf{R}}[k] = A_f y_{\mathsf{R}}[k] \,. \tag{57}$$

The received signals at the two destinations in phase 2 are

$$\tilde{y}_{1}[k] = A_{f}G_{1}[k]y_{R}[k] + \tilde{\eta}_{1}[k]
= A_{f}G_{1}[k]H_{R}[k]x_{S}[k] + \tilde{\eta}'_{1}[k],$$
(58)

$$\tilde{y}_{2}[k] = A_{f}G_{2}[k]y_{R}[k] + \tilde{\eta}_{2}[k]
= A_{f}G_{2}[k]H_{R}[k]x_{S}[k] + \tilde{\eta}'_{2}[k],$$
(59)

where

$$\tilde{\eta}_1'[k] = A_f G_1[k] \eta_R[k] + \tilde{\eta}_1[k], \tag{60}$$

$$\tilde{\eta}_{2}'[k] = A_{f}G_{2}[k]\eta_{R}[k] + \tilde{\eta}_{2}[k].$$
 (61)

Define two constants

$$c_1^2 = 1 + \Gamma_R + \tilde{\Gamma}_1, \tag{62}$$

$$c_2^2 = 1 + \Gamma_R + \tilde{\Gamma}_2. \tag{63}$$

Assuming that the noise terms $\eta_R[k]$ and $\tilde{\eta}_1[k]$ are independent, the equivalent noise $\tilde{\eta}_1'[k]$ is zero-mean, complex Gaussian with variance

$$\mathbb{E}[|\tilde{\eta}_{1}'[k]|^{2}] = \sigma^{2}(1 + A_{f}^{2}\mathbb{E}[|G_{1}[k]|^{2}]) = c_{1}^{2}\sigma^{2}.$$
 (64)

Similarly for $\eta'_2[k]$, we have

$$\mathbb{E}\Big[|\tilde{\eta}_{2}'[k]|^{2}\Big] = \sigma^{2}\Big(1 + A_{f}^{2}\mathbb{E}[|G_{2}[k]|^{2}]\Big) = c_{2}^{2}\sigma^{2}.$$
 (65)

For U_1 , the output of the MRC detector is

$$z_1[k] = w_{11}[k]y_1[k] + w_{12}[k]\tilde{y}_1[k], \tag{66}$$

where $w_{11}[k]$ and $w_{12}[k]$ are the weights and determined as

$$w_{11}[k] = \frac{\sqrt{\alpha P_{\rm S}} H_1^*[k]}{\tilde{\alpha} P_{\rm S} |H_1[k]|^2 + \sigma^2},\tag{67}$$

$$w_{12}[k] = \frac{A_f \sqrt{\alpha P_{\rm S}} H_{\rm R}^*[k] G_1^*[k]}{A_f^2 \bar{\alpha} P_{\rm S} |H_{\rm R}[k]|^2 |G_1[k]|^2 + c_1^2 \sigma^2}.$$
 (68)

The instantaneous SINR at U_1 is

$$\gamma_1^{AF}[k]$$

$$= \frac{\alpha P_{\rm S} |H_1[k]|^2}{\tilde{\alpha} P_{\rm S} |H_1[k]|^2 + \sigma^2} + \frac{A_f^2 \alpha P_{\rm S} |H_{\rm R}[k]|^2 |G_1[k]|^2}{A_f^2 \tilde{\alpha} P_{\rm S} H_{\rm R}[k]|^2 |G_1[k]|^2 + c_1^2 \sigma^2}$$
(69)

$$= \frac{\alpha}{\bar{\alpha} + \frac{1}{\gamma_1[k]}} + \frac{\alpha}{\bar{\alpha} + \frac{c_1^2}{\gamma_R[k]\bar{\gamma}_1[k]}}.$$
 (70)

Hence, the instantaneous mutual information between S and U_1 at the kth subcarrier is

$$\mathcal{F}_{1}[k] = \frac{1}{2}\log_{2}(1 + \gamma_{1}^{AF}[k])$$

$$= \frac{1}{2}\log_{2}\left(1 + \frac{\alpha}{\bar{\alpha} + \frac{1}{\gamma_{1}[k]}} + \frac{\alpha}{\bar{\alpha} + \frac{c_{1}^{2}}{\gamma_{R}[k]\bar{\gamma}_{1}[k]}}\right).$$
(71)

 U_2 will first decode the first data stream and subtract the contribution from the received signal. Under the assumption that decoding done successfully, we obtain

$$y_2^{\Delta}[k] = \sqrt{\bar{\alpha}P_8}H_2[k]x_2[k] + \eta_2[k], \tag{72}$$

$$\tilde{y}_{2}^{\Delta}[k] = A_{f}\sqrt{\bar{\alpha}P_{S}}G_{2}[k]H_{R}[k]x_{2}[k] + \tilde{\eta}_{2}'[k]. \tag{73}$$

Based on these data streams, U_2 applies MRC to obtain

$$z_2[k] = w_{21}[k]y_2^{\Delta}[k] + w_{22}[k]\tilde{y}_2^{\Delta}[k], \tag{74}$$

where the weights are

$$w_{21}[k] = \frac{\sqrt{\bar{\alpha}P_{\rm s}}H_2^*[k]}{\sigma^2},\tag{75}$$

$$w_{22}[k] = \frac{A_f \sqrt{\bar{\alpha} P_{\rm S}} H_{\rm R}^*[k] G_2^*[k]}{c_2^2 \sigma^2} \,. \tag{76}$$

The instantaneous SNR at U_2 is

$$\gamma_2^{\text{AF}}[k] = \frac{\bar{\alpha} P_{\text{S}} |H_2[k]|^2}{\sigma^2} + \frac{A_f^2 \bar{\alpha} P_{\text{S}} |H_{\text{R}}[k]|^2 |G_2[k]|^2}{c_2^2 \sigma^2}$$
(77)

$$= \bar{\alpha}\gamma_2[k] + \frac{\bar{\alpha}}{c_2^2}\gamma_R[k]\tilde{\gamma}_2[k]. \tag{78}$$

Hence, the instantaneous mutual information between S and U_2 at the kth subcarrier is

$$\mathcal{I}_{2}[k] = \frac{1}{2}\log_{2}\left(1 + \gamma_{2}^{AF}[k]\right)$$

$$= \frac{1}{2}\log_{2}\left(1 + \tilde{\alpha}\gamma_{2}[k] + \frac{\tilde{\alpha}}{c_{2}^{2}}\gamma_{R}[k]\tilde{\gamma}_{2}[k]\right).$$
(79)

The mutual information for U_1 and U_2 averaged over all data subcarriers can be found using (31).

4.1 Average mutual information for U_1

Following the same procedure and assumptions adopted for the DF scheme. From (71), the average mutual information for U_1 is

$$\bar{\mathcal{J}}_1 = \mathbb{E}[\mathcal{J}_1[k]] = \frac{1}{2\ln 2} \mathbb{E}[\ln(1+A+D)],\tag{80}$$

where A is defined in (35) and

$$D = \frac{\alpha}{\bar{\alpha} + \frac{c_1^2}{r_0 \bar{\gamma}}}.$$
(81)

Using (36), we have

$$\bar{\mathcal{J}}_{1} = \frac{1}{2\ln 2} \mathbb{E} \left[\int_{0}^{\infty} \frac{1}{y} (e^{-y} - e^{-(1+A+D)y}) dy \right]$$
 (82)

$$= \frac{1}{2\ln 2} \int_{0}^{\infty} \frac{1}{y} (e^{-y} - e^{-y} \mathbb{E}[e^{-Ay}] \mathbb{E}[e^{-Dy}]) dy.$$
 (83)

 $\mathbb{E}[e^{-Ay}]$ is found in (39). To find $\mathbb{E}[e^{-Dy}]$, define $\gamma_z = \gamma_R \tilde{\gamma}_1$, the product of two independent exponential random variables. Hence, it has the distribution

$$f(\gamma_z) = \frac{2}{\Gamma_0 \tilde{\Gamma}_1} K_0 \left[2 \sqrt{\frac{\gamma_z}{\Gamma_0 \tilde{\Gamma}_1}} \right], \tag{84}$$

where $K_0[.]$ is the modified Bessel function of the second kind [55]. Subsequently,

$$\mathbb{E}\left[e^{-Dy}\right] = \int_0^\infty e^{\left(-\frac{\alpha y}{\tilde{\alpha} + \frac{c_1^2}{\gamma_z}}\right)} \frac{2}{\Gamma_R \tilde{\Gamma}_2} K_0 \left[2\sqrt{\frac{\gamma_z}{\Gamma_R \tilde{\Gamma}_2}}\right] d\gamma_z. \tag{85}$$

Inserting (39) and (85) into (82), we get the average mutual information \mathcal{J}_1 . A two-dimensional integration is needed for numerical evaluations.

4.2 Average mutual information for U_2

From (79), the average mutual information for U_2 will be

$$\bar{\mathcal{J}}_2 = \mathbb{E}[\mathcal{J}_2] = \frac{1}{2\ln 2} \mathbb{E}[\ln(1+Q+N)],\tag{86}$$

where

$$Q = \tilde{\alpha}\gamma_2, \quad N = \frac{\tilde{\alpha}}{c_2^2}\gamma_R\tilde{\gamma}_2. \tag{87}$$

Again, using (36), we obtain

$$\bar{\mathcal{J}}_{2} = \frac{1}{2\ln 2} \mathbb{E} \left[\int_{0}^{\infty} \frac{1}{y} \left(e^{-y} - e^{-(1+Q+N)y} \right) dy \right]$$
 (88)

$$= \frac{1}{2\ln 2} \int_{0}^{\infty} \frac{1}{y} (e^{-y} - e^{-y} \mathbb{E}[e^{-Qy}] \mathbb{E}[e^{-Ny}]) dy.$$
 (89)

Since $Q = \bar{\alpha}\gamma_2$, we have

$$\mathbb{E}\left[e^{-Qy}\right] = \frac{1}{1 + \bar{\alpha}\Gamma_2 y}.$$
 (90)

To find $\mathbb{E}[e^{-Ny}]$, we define $\gamma_w = \gamma_R \tilde{\gamma}_2$, which leads to

$$\mathbb{E}\left[e^{-Ny}\right] = \int_0^\infty e^{\left(-\frac{\tilde{\alpha}}{c_2^2}\gamma_w y\right)} \frac{2}{\Gamma_R \tilde{\Gamma}_2} K_0 \left[2\sqrt{\frac{\gamma_w}{\Gamma_R \tilde{\Gamma}_2}}\right] d\gamma_w. \tag{91}$$

Inserting (90) and (91) into (88), we get the average mutual information $\bar{\mathcal{J}}_2$. A two-dimensional integration is needed for numerical evaluations.

4.3 The boundary of the achievable ergodic rate region

Having found the average mutual information for U_1 and U_2 in Sections 4.1 and 4.2 for a given value of α , the ergodic rate region is given by

$$\left\{ \bigcup \left[R_1 \le \bar{\mathcal{J}}_1, R_2 \le \bar{\mathcal{J}}_2 \right] \right\}, \tag{92}$$

where the boundary of the achievable rate region can be obtained by varying the value of α .

4.4 Outage probability for a given rate pair

For a finite K, the outage probability is defined according to (45). Unlike the DF scheme, R always forwards the data it received. Hence, the outage probability at U_1 is

$$p_{1}^{\text{out}}(R_{1}^{*}) = \mathbb{P}\left\{\frac{1}{K_{d}} \sum_{k \in K_{d}} \frac{1}{2} \log_{2}(1 + \gamma_{1}^{\text{AF}}[k]) < R_{1}^{*}\right\}, \tag{93}$$

where $\gamma_1^{AF}[k]$ is given by (69). The outage probability at U_2 is

$$p_{2}^{\text{out}}(R_{2}^{*}) = 1 - \mathbb{P}\left\{\frac{1}{K_{d}} \sum_{k \in K_{d}} \frac{1}{2} \log_{2} \left(1 + \gamma_{1 \to 2}^{AF}[k]\right) \ge R_{1}^{*}\right\}$$

$$\bigcap \frac{1}{K_{d}} \sum_{k \in K_{d}} \frac{1}{2} \log_{2} \left(1 + \gamma_{2}^{AF}[k]\right) \ge R_{2}^{*},$$
(94)

where $\gamma_2^{AF}[k]$ is given by (77) and

$$\gamma_{1 \to 2}^{AF}[k] = \frac{\alpha P_{S} |H_{2}[k]|^{2}}{\tilde{\alpha} P_{S} |H_{2}[k]|^{2} + \sigma^{2}} + \frac{A_{f}^{2} \alpha P_{S} |H_{R}[k]|^{2} |G_{2}[k]|^{2}}{A_{f}^{2} \tilde{\alpha} P_{S} H_{R}[k]|^{2} |G_{2}[k]|^{2} + c_{1}^{2} \sigma^{2}}.$$
(95)

4.5 System operation

One can see that the outage probabilities depend on α . Like the DF scheme, we here adopt an *ad-hoc* approach to find α using the results from the ergodic rate region. Given a target rate pair, one can find the corresponding operating point on the boundary of the ergodic rate region and the corresponding α . Let $\lambda = R_2^*/R_1^*$ denote the target rate ratio. With the knowledge of statistical CSI, the power fraction under the given target rate pair is obtained via

$$\hat{\alpha}_{AF} = \arg\min_{\alpha} \left| \frac{\bar{R}_2}{\bar{R}_1} - \lambda \right|,$$
 (96)

where (\bar{R}_1, \bar{R}_2) is the point on the boundary of the ergodic rate region.

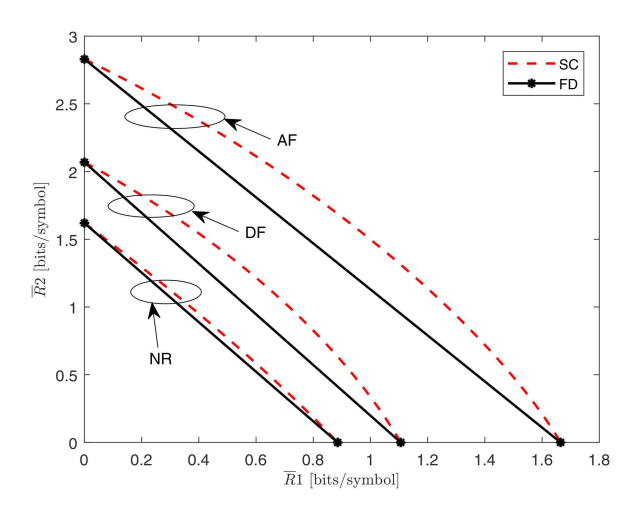


Fig. 2 Boundaries of the achievable rate regions of the DF, AF, and NR schemes under FD and SC at $\Gamma_{\rm ref}=10$ dB when $d_{\rm SR}=0.5$ km

5 Simulation results

In this section, we will first determine the boundaries of the achievable rate regions the DF, AF, and NR schemes under FD and SC. Then we will investigate the outage probabilities at the two users as R is moving away from S. Finally, we will compare the performance of FD and SC in terms of outage probability. It's assumed that the distances among the nodes, as shown in Fig. 1, are $d_{\rm SU_1}=1.7$ km, $d_{\rm SU_2}=1.3$ km, $d_{\rm RU_1}=0.94$ km, and $d_{\rm RU_2}=0.54$ km, while $d_{\rm SR}$ varies from 0.25 to 1.25 km.

The number of OFDM subcarriers is K = 1024 with $K_{\rm d} = 672$ and the number of channel taps on every channel is L = 32. The target rates, R_1^* and R_2^* , are set to 1 bit/symbol, and we choose the average SNR of longest link, Γ_1 , to be $\Gamma_{\rm ref}$. Moreover, in our simulations, the outage at R is considered.

It is widely accepted that

$$\mathbb{E}\left\{\left|H[k]\right|^{2}\right\} \propto (d/d_{0})^{-n} \tag{97}$$

where H[k] is the frequency response at a receiver d metres away from the transmitter, d_0 is the reference distance, and n is the path loss exponent and it's between 2.7 and 3.5 for urban cellular area. Hence, we set n = 3.

5.1 Boundaries of the achievable rate region

We now evaluate the boundaries of the achievable rate regions of the DF, AF, and NR schemes under FD and SC. The regions of the DF and AF schemes under SC are based on (44) and (92), respectively. Under FD, they are based on [41, eq. (16)].

According to the system setup, R could be located at different locations. For the purpose of demonstration, we picked two distances, $d_{\rm SR}=0.5$ km and $d_{\rm SR}=1$ km. From Figs. 2 and 3, it can be observed that the DF scheme has the best achievable ergodic rate region compared to the AF and NR schemes if $d_{\rm SR}=1$ km. However, the AF scheme offers the best region when $d_{\rm SR}=0.5$ km, i.e., R is closer to S. On the other hand, SC always has the larger achievable ergodic rate regions compared to FD. This can be explained as follows: SC gives the near user U_2 a complete degree of freedom while being allocated only a small amount of transmit power, thus, causing a small amount of interference to the far user U_1 . Therefore, both users can achieve reasonable rates. On the contrary, FD allocates a significant fraction of the bandwidth to U_1 to achieve the same performance as for U_2 which causes a large degradation in the performance of U_2 .

5.2 Outage probability at different relay locations

We next study the effect of changing the location of R in the network on the outage probabilities at the two users. Figs. 4 and 5 show the outage probabilities of the two users for the DF and AF

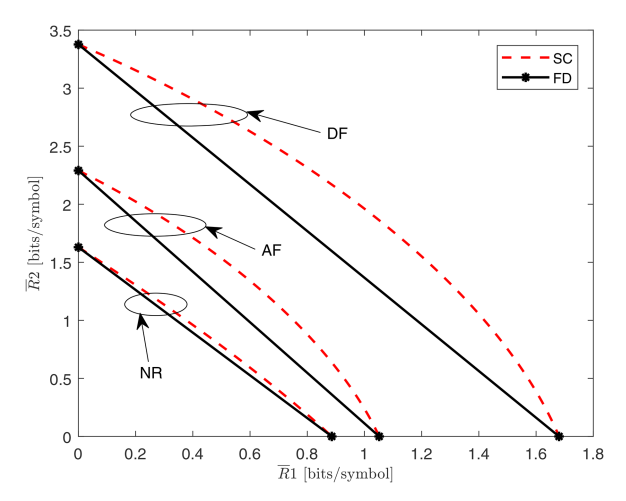


Fig. 3 Boundaries of the achievable rate regions of the DF, AF, and NR schemes under FD and SC at $\Gamma_{\rm ref}=10$ dB when $d_{\rm SR}=1$ km

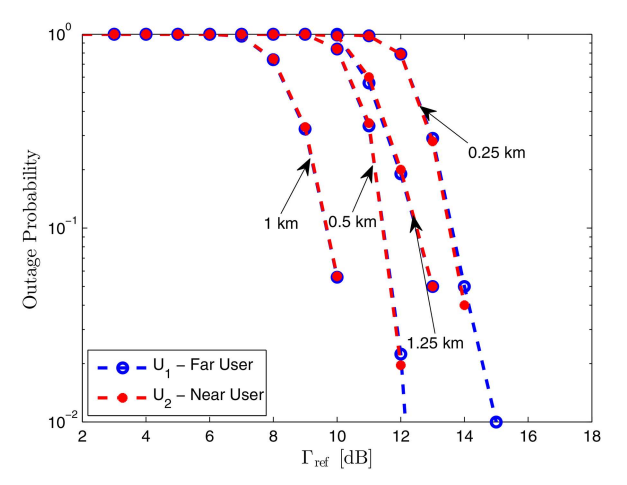


Fig. 4 DF at different d_{SR}

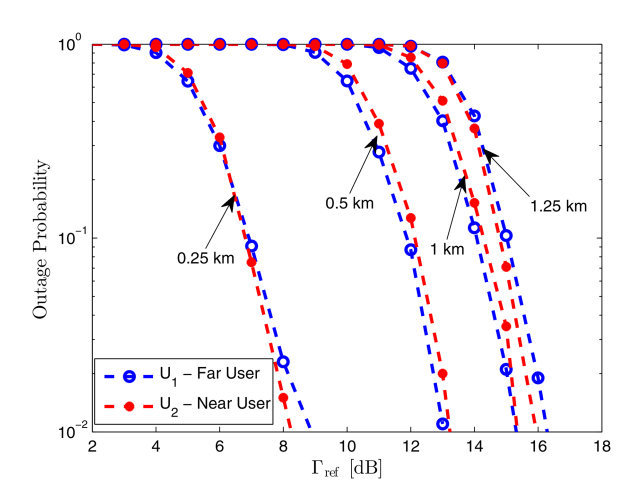


Fig. 5 AF at different d_{SR}

schemes at different distances $d_{\rm SR}$, respectively. For the DF scheme, we can notice that the lowest outage probability happens when $d_{\rm SR}=1$ km. Moreover, this outage probability is getting larger when R is either near or far away from S. In the latter one, this corresponds to be near to the users. On the other hand, for the AF scheme, as R is moving away from S, the outage probability is getting larger. This makes sense as the AF scheme simply amplifies the received signal with the included noise which increases as R is moving away from S. As R is moving towards S, it will act as a repeater which helps the two users to perform better than the NR and DF schemes.

It's worth to point out here that the optimum parameters at the two picked distances are as follows: $\alpha_{\rm DF} = 0.82$, $\beta_{\rm DF} = 0.85$, and

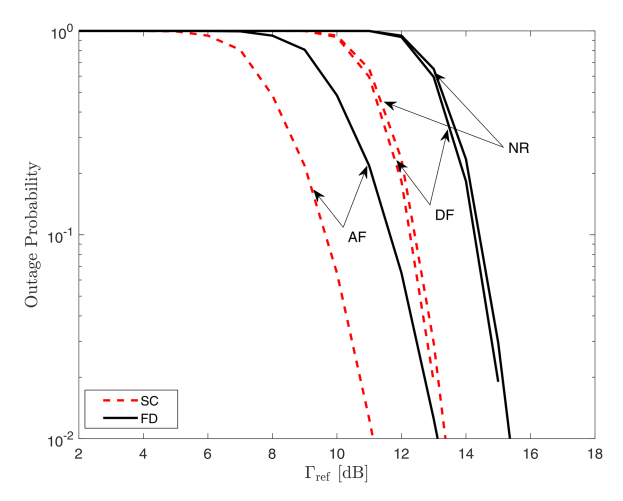


Fig. 6 Comparison between FD and SC with different relay schemes when $d_{\rm SR}=0.5~{\it km}$

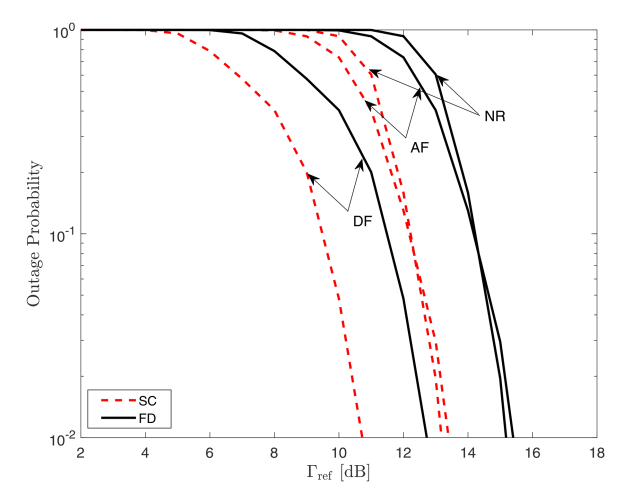


Fig. 7 Comparison between FD and SC with different relay schemes when $d_{\rm SR}=1~{\rm km}$

 $\alpha_{AF} = 0.87$ at $d_{SR} = 0.5$ km. However, $\alpha_{DF} = 0.88$, $\beta_{DF} = 0.89$, and $\alpha_{AF} = 0.89$ at $d_{SR} = 1$ km. While, $\alpha_{NR} = 0.79$.

5.3 Comparison between FD and SC

To complete the picture, we compare the performance of FD with SC under the three relay options. To make it easier for reading, we plot the average outage probability at the two users instead of plotting each user's outage probability. Figs. 6 and 7 show the outage probabilities when $d_{\rm SR}=0.5\,{\rm km}$ and $d_{\rm SR}=1\,{\rm km}$, respectively. From these figures, we can see that SC is always better than FD regardless the scheme is used or where R is. However, the DF scheme is the best at $d_{\rm SR}=1\,{\rm km}$ but the AF scheme is the best when R is near S.

6 Conclusion

We investigated superposition coded OFDM transmissions in a downlink cooperative relay network where the source splits the power between two users based on statistical CSI under either the DF or AF scheme. We derived the ergodic rate regions, from which, the power splitting parameters can be specified when the target data rates are given. Results of outage probabilities show that SC is always better than FD regardless the relay scheme is adopted or where the relay is located. However, when it comes it to decide which scheme to use, the DF or AF scheme, the relay location is the dominant factor.

References

- Dai, L., Wang, B., Yuan, Y., et al.: 'Non-orthogonal multiple access for 5G: Solutions, challenges, opportunities, and future research trends', *IEEE Commun. Mag.*, 2015, **53**, (9), pp. 74–81
 Wei, Z., Yuan, J., Ng, D.W.K., *et al.*: 'A survey of downlink non-orthogonal multiple access for 5G wireless communication networks', *ZTE Commun.*,
- [2] 2016, 14, (4), pp. 17-26
- Liu, Y., Ding, Z., Elkashlan, M., et al.: 'Cooperative non-orthogonal multiple [3] access with simultaneous wireless information and power transfer', IEEE J.
- Sel. Areas Commun., 2016, 34, (4), pp. 938–953
 Ding, Z., Lei, X., Karagiannidis, G.K., et al.: 'A survey on non-orthogonal multiple access for 5G networks: research challenges and future trends', IEEE [4] J. Sel. Areas Commun., 2017, **35**, (10), pp. 2181–2195
- Shin, W., Vaezi, M., Lee, B., et al.: 'Non-orthogonal multiple access in multi-[5] cell networks: theory, performance, and practical challenges', IEEE Commun. Mag., 2017, 55, (10), pp. 176-183
- Islam, S.M., Zeng, M., Dobre, O.A.: 'NOMA in 5G systems: Exciting [6] possibilities for enhancing spectral efficiency'. 2017, arXiv e-prints Cover, T.M., Thomas, J.A.: 'Elements of information theory' (John Wiley &
- [7] Sons, Inc., NJ, 2006, 2nd edn.)
- Benjebbour, A., Li, A., Saito, Y., et al.: 'System-level performance of [8] downlink NOMA for future LTE enhancements'. Proc. IEEE Globecom Workshops (GC Wkshps), Atlanta, GA, USA, December 2013, pp. 66–70
- Saito, Y., Benjebbour, A., Kishiyama, Y., et al.: 'System-level performance evaluation of downlink non-orthogonal multiple access (NOMA)'. Proc. of [9] IEEE Int. Symp. on Personal Indoor and Mobile Radio Communications (PIMRC), London, UK, September 2013, pp. 611-615
- Tabassum, H., Ali, M.S., Hossain, E., et al.: 'Non-orthogonal multiple access (NOMA) in cellular uplink and downlink: Challenges and enabling techniques', 2016, arXiv e-prints
 Saito, Y., Kishiyama, Y., Benjebbour, A., et al.: 'Non-orthogonal multiple
- [11] access (NOMA) for cellular future radio access'. Proc. IEEE Vehicular Technology Conf. (VTC Spring), Dresden, Germany, June 2013, pp. 1–5 Lan, Y., Benjebboiu, A., Chen, X., et al.: 'Considerations on downlink non-
- [12] orthogonal multiple access (NOMA) combined with closed-loop SU-MIMO'. Proc. IEEE Int. Conf. on Signal Processing and Communication Systems (ICSPCS), Gold Coast, Australia, December 2014, pp. 1–5 Chen, X., Benjebbour, A., Lan, Y., et al.: 'Impact of rank optimization on
- [13] downlink non-orthogonal multiple access (NOMA) with SU-MIMO'. Proc. IEEE Int. Conf. on Communication Systems (ICCS), Macau, China, November 2014, pp. 233–237
- Sun, Q., Han, S., Xu, Z., et al.: 'Sum rate optimization for MIMO nonorthogonal multiple access systems'. Proc. IEEE Wireless Communications and Networking Conf. (WCNC), New Orleans, LA, USA, March 2015, pp. 747–752
- Choi, J.: 'Minimum power multicast beamforming with superposition coding [15] for multiresolution broadcast and application to NOMA systems', IEEE Trans. Commun., 2015, 63, (3), pp. 791-800
- Sun, Q., Han, S., Chin-Lin, I., et al.: 'On the ergodic capacity of MIMO [16] NOMA systems', *IEEE Wirel. Commun. Lett.*, 2015, **4**, (4), pp. 405–408 Hanif, M.F., Ding, Z., Ratnarajah, T., *et al.*: 'A minorization-maximization
- [17] method for optimizing sum rate in the downlink of non-orthogonal multiple access systems', *IEEE Trans. Signal Process.*, 2016, **64**, (1), pp. 76–88
- Ding, Z., Schober, R., Poor, H.V.: 'A general MIMO framework for NOMA downlink and uplink transmission based on signal alignment', IEEE Trans. Wirel. Commun., 2016, 15, (6), pp. 4438–4454
 Ding, Z., Liu, Y., Choi, J., et al.: 'Application of non-orthogonal multiple
- [19] access in LTE and 5G networks', IEEE Commun. Mag., 2017, 55, (2), pp.
- [20] Laneman, J.N., Tse, D.N., Wornell, G.W.: 'Cooperative diversity in wireless networks: efficient protocols and outage behavior', IEEE Trans. Inf. Theory, 2004, **50**, (12), pp. 3062–3080
- [21]
- Ding, Z., Peng, M., Poor, H.V.: 'Cooperative non-orthogonal multiple access in 5G systems', *IEEE Commun. Lett.*, 2015, **19**, (8), pp. 1462–1465

 Nonaka, N., Kishiyama, Y., Higuchi, K.: 'Non-orthogonal multiple access using intra-beam superposition coding and SIC in base station cooperative [22] MIMO cellular downlink', IEICE Trans. Commun., 2015, 98, (8), pp. 1651-
- [23] Kim, J.B., Lee, I.H.: 'Capacity analysis of cooperative relaying systems using non-orthogonal multiple access', IEEE Commun. Lett., 2015, 19, (11), pp.
- Xu, Y., Sun, H., Hu, R.Q., et al.: 'Cooperative non-orthogonal multiple access [24] in heterogeneous networks'. Proc. IEEE Global Communications Conf. (GLOBECOM), San Diego, CA, USA, December 2015, pp. 1-6
- Men, J., Ge, J.: 'Performance analysis of non-orthogonal multiple access in downlink cooperative network', IET Commun., 2015, 9, (18), pp. 2267–2273
- [26] Xu, M., Ji, F., Wen, M., et al.: 'Novel receiver design for the cooperative relaying system with non-orthogonal multiple access', *IEEE Commun. Lett.*, 2016, **20**, (8), pp. 1679–1682

- [27] Ding, Z., Dai, H., Poor, H.V.: 'Relay selection for cooperative NOMA', IEEE Wirel. Commun. Lett., 2016, 5, (4), pp. 416–419 Liu, Y., Pan, G., Zhang, H., et al.: 'Hybrid decode-forward & amplify-forward
- relaying with non-orthogonal multiple access', IEEE Access, 2016, 4, pp.
- Men, J., Ge, J., Zhang, C.: 'Performance analysis of nonorthogonal multiple access for relaying networks over Nakagami-m fading channel', IEEE Trans.
- Luo, S., Teh, K.C.: 'Adaptive transmission for cooperative NOMA system with buffer-aided relaying', *IEEE Commun. Lett.*, 2017, 21, (4), pp. 937–940 Liang, X., Wu, Y., Ng, D.W.K., et al.: 'Outage performance for cooperative NOMA transmission with an AF relay', *IEEE Commun. Lett.*, 2017, 21, (11), pp. 2428-2431
- [32] Zhong, C., Zhang, Z.: 'Non-orthogonal multiple access with cooperative fullduplex relaying', *IEEE Commun. Lett.*, 2016, **20**, (12), pp. 2478–2481 Zhang, Z., Ma, Z., Xiao, M., *et al.*: 'Full-duplex device-to-device-aided
- [33] cooperative nonorthogonal multiple access', IEEE Trans. Veh. Technol., 2017, **66**, (5), pp. 4467–4471
- Zhang, L., Liu, J., Xiao, M., et al.: 'Performance analysis and optimization in downlink NOMA systems with cooperative full-duplex relaying', IEEE J. Sel. Areas Commun., 2017, 35, (10), pp. 2398-2412
- Gerzaguet, R., Bartzoudis, N., Baltar, L., et al.: 'The 5G candidate waveform [35] race: a comparison of complexity and performance', *EURASIP J. Wirel. Commun. Netw.*, 2017, **1**, (13), pp. 13

 Jebbar, H., El Hassani, S., El Abbassi, A.: 'Performance study of 5G multicarrier waveforms'. Proc. IEEE Int. Conf. on Wireless Networks and
- Mobile Communications (WINCOM), Rabat, Morocco, 2017, pp. 1-6
- [37] Cai, Y., Qin, Z., Cui, F., et al.: 'Modulation and multiple access for 5G networks', IEEE Commun. Surv. Tutor., Firstquarter 2018, 20, (1), pp. 629-
- [38] Parida, P., Das, S.S.: 'Power allocation in OFDM based NOMA systems: a DC programming approach'. Proc. IEEE Globecom Workshops (GC Wkshps), Austin, TX, USA, December 2014, pp. 1026-1031
- Li, X., Li, C., Jin, Y.: 'Dynamic resource allocation for transmit power minimization in OFDM-based NOMA systems', IEEE Commun. Lett., 2016,
- **20**, (12), pp. 2558–2561 Cai, W., Chen, C., Bai, L., *et al.*: 'Subcarrier and power allocation scheme for [40] downlink OFDM-NOMA systems', IET Signal Process., 2016, 11, (1), pp.
- Ma, L., Zhou, S., Qiao, G., et al.: 'Superposition coding for downlink underwater acoustic OFDM', *IEEE J. Ocean. Eng.*, 2017, **42**, (1), pp. 175– [41]
- Gokceli, S., Kurt, G.K.: 'Superposition coded-orthogonal frequency division multiplexing', $I\!E\!E\!E\!Access$, 2018, 6, pp. 14842–14856 [42]
- Ding, Z., Fan, P., Poor, H.V.: 'Impact of user pairing on 5G nonorthogonal multiple-access downlink transmissions', IEEE Trans. Veh. Technol., 2016, **65**, (8), pp. 6010–6023
- Tse, D.N.: 'Optimal power allocation over parallel Gaussian broadcast channels'. Proc. IEEE Int. Symp. on Information Theory, Ulm, Germany, July 1997, p. 27
- Li, L., Goldsmith, A.J.: 'Capacity and optimal resource allocation for fading [45] broadcast channels. I. Ergodic capacity', IEEE Trans. Inf. Theory, 2001, 47,
- Li, L., Goldsmith, A.J.: 'Capacity and optimal resource allocation for fading broadcast channels. II. outage capacity', IEEE Trans. Inf. Theory, 2001, 47, (3), pp. 1103-1127
- [47] 3GPP RP-160680: 'Downlink multiuser superposition transmissions for LTE'. Tech. Rep., March, 2016
- Lee, H., Kim, S., Lim, J.H.: 'Multiuser superposition transmission (MUST) for LTE-A systems'. Proc. IEEE Int. Conf. on Communications (ICC), Kuala Lumpur, Malaysia, May 2016, pp. 1-6
- Cover, T.M.: 'Broadcast channels', IEEE Trans. Inf. Theory, 1972, 18, (1), pp. [49] 2-14
- Vanka, S., Srinivasa, S., Gong, Z., et al.: 'Superposition coding strategies: design and experimental evaluation', *IEEE Trans. Wirel. Commun.*, 2012, 11, [50] (7), pp. 2628–2639
- [51] Simon, M.K., Alouini, M.S.: 'Digital communication over fading channels', vol. 95 (John Wiley & Sons, NJ, 2005)
- Goldsmith, A.J.: 'Wireless communications' (Cambridge University Press, NY. 2005)
- [53] Abramowitz, M., Stegun, I.A.: 'Handbook of mathematical functions: with formulas, graphs, and mathematical tables', vol. 55 (Courier Corporation, MA, 1964)
- Papoulis, A., Pillai, S.U.: 'Probability, random variables, and stochastic processes' (McGraw Hill, NY, 2002, 4th edn.)
- [55] Gradshteyn, I.S., Ryzhik, I.M.: 'Table of integrals, series, and products' (Academic Press, MA, 2000, 6th edn.)